ELSEVIER

Energy and Buildings 24 (1996) 183–194

ENERGY AND BUILDINGS

A quasi-steady-state model of attic heat transfer with radiant barriers

David W. Winiarski [a], Dennis L. O'Neal [b]

[a] *Battelle Pacific Northwest Laboratory, Richland, WA 99352, USA*

[b] *Department of Mechanical Engineering, Texas A&M University, College Station, TX 77843-3123, USA*

Received 10 October 1993; revised 28 March 1996

Abstract

During the cooling season, heat transfer from the attic into the conditioned space of a residence can represent a significant portion of the total envelope heat transfer. Radiant barriers are one method used to reduce this heat transfer. A quasi-steady-state model was developed for predicting attic heat transfer in residences with radiant barrier systems. The model was used to estimate the reduction in cooling load that would occur with a radiant barrier and to identify important construction and environmental parameters that influence this cooling load reduction. The model's output consisted of hourly ceiling heat fluxes inside the house based on hourly weather data inputs. Model results were compared with detailed experimental results from two small test houses. The model predicted typical summer heat flux reductions of between 35 and 43% with different radiant barrier configurations and levels of insulation. These compared to measured heat flux reductions of between 29 and 37% in attics under the same conditions. Sensitivity studies were also conducted to show the effect of uncertainty in several of the important physical attic parameters on the final heat flow predictions of the model.

Keywords: Residential buildings; Envelope; Heat transfer; Computer simulation; Radiant barrier

1. Introduction

Radiant barriers are designed to reduce the radiant heat transfer that occurs between the roof deck and attic floor of a residence or commercial building. Radiant barriers are thin sheets of material having at least one low-emissivity surface. Typically, this is an aluminized foil surface bonded to paper, plastic or a reinforcing mesh for strength. The emissivity of the clean foil surface is typically less than 0.05. The barrier is placed in the attic with the low-emissivity surface facing the attic airspace. The average distance between roof deck and attic floor typically varies between 1 and 3 m in most residential buildings. Because of this, thermal radiation is the primary method of heat transfer between a hot roof deck and the attic floor. Because the heated attic air tends to stratify next to the roof deck, natural convection can usually play only a minor role in removing heat from the roof deck. The radiation blockage obtained through the use of a radiant barrier can dramatically reduce the radiant heat transfer across this airspace and thus also reduce the heat transferred to the living space.

At each attic surface, there is a complicated interplay between the heat that is conducted, radiated or convected to that surface. During daytime periods in the cooling season, heat is radiated from the roof deck downwards to the attic floor and then either convected upwards from the floor into the attic ventilating air or conducted down to the living space below. The net impact of a radiant barrier on the heat conducted into the living space depends on such variables as the conditioned space temperature, ambient air temperature, ventilation rate, solar insolation, and the absorptivities, emissivities and thermal resistances of the other attic surfaces. Accurate modeling of attic heat transfer allows prediction of the impact or radiant barriers under varying conditions.

Modeling work on attic heat transfer and radiant barrier systems began with a single, steady-state equation developed by Joy [1]. This equation assumed a flat roof and required constant values for the ventilation rate, all convection coefficients and all radiative heat transfer coefficients. The work by Joy forms the basis of the tables for effective attic resistance suggested by ASHRAE [2]. Peavy [3] developed a computer model to predict ceiling heat transfer in residential attics under different ventilation conditions. Peavy's model calculated the transient heat flow using conduction transfer functions for three attic surfaces, two roof sections and the attic floor. The gable ends were assumed to be refractory surfaces. An average sol–air temperature was used to calculate the roof temperature, and an average attic air temperature was used in calculating the heat convected to the attic ventilating air. Wilkes [4] expanded upon Peavy's model to

PII S0378-7788(96)00987-5

include heat transfer through all attic surfaces, moisture transfer effects inside the attic, and physical calculation of the estimated ventilation rate. The model also incorporated an additional ventilated airspace between a truss radiant barrier and the roof deck when the truss radiant barrier was modeled. Fairey et al. developed a simplified steady-state model using a flat roof and two attic air zones [5,6]. This model calculated a single air temperature for the lower air zone using a heat balance between the heat convected between the attic floor and the lower air zone and the temperature rise between the outdoor air and lower air zone temperature. This differed from the more complicated exponential temperature rise for air moving across the attic floor that was considered by Joy in his steady-state equation. The simple, two-zone model of Fairey et al. gave ceiling heat fluxes similar to that measured by Joy under the same set of conditions for the flat roof model. A one-zone model structured similarly was seen to consistently overestimate the ceiling heat flux, particularly with the radiant barrier in place. Parametric studies using the model could not show any difference between the roof-mounted or the floor-mounted radiant barrier. The effects of varying the ventilation rate, ambient air temperature and radiant barrier emissivity were examined for a constant sol–air temperature of 71°C (160°F). The model suggested that attic ventilation beyond a rate of 0.076 $m^3/(min\ m^2)$ (0.25 cfm/ft^2) had little effect on the percentage heat flux reduction. The model was also sensitive to radiant barrier emissivity and inlet air temperature for all the cases examined.

This paper describes the development of a quasi-steady-state model used to calculate heat transfer at all attic surfaces. The model incorporated a two-zone model of air flow. The model includes provisions for three different placements of radiant barriers in a residential attic. Although the model relied on steady-state heat calculations at every hour, it utilizes results from a transient finite difference analysis that indicated that typical time delays of one hour were appropriate for the insulation in attics. Comparisons between the model predictions and experimental test results are also provided.

2. Attic structure and physical parameters

The attic assumed a five-sided enclosure consisting of two attic gables, two roof sections and the attic floor. The attic floor is defined as the upper surface of the ceiling insulation. Each surface was modeled as a flat, diffusely emitting plane with a constant emissivity with respect to temperature. The temperature of each surface was also assumed not to vary spatially across the surface. It was recognized that the attic rafters supporting the roof sections would have some effect on both the radiation and convection of energy from the roof deck. The effect on convection would be largely dependent on the air flow pattern inside the attic. Rafters or trusses support the attic by running from the edge of the roof to the ridge beam as seen in Fig. 1. During a hot summer day, air heated by convection from the roof deck rises along this slope. A layer of heated air remains near the attic deck, the presence of the rafters resisting the removal of that layer of heated air by attic crossflow ventilation.

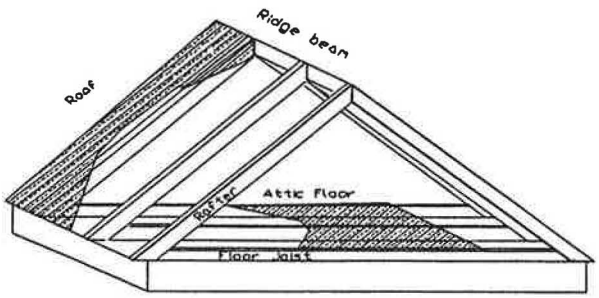

Fig. 1. Construction components of an attic.

The effect of the rafters on the radiative heat transfer could be significant. To account for the blockage of radiation to the rafters, the side of each rafter was treated as an adiabatic re-radiating surface, as suggested by the symmetry of the attic rafter placement. Heat conduction from the roof to the bottom surface of each rafter was treated as one-dimensional and was assumed not to interact with heat radiating from the sides of the rafter. Each roof section was approximated as an infinitely long surface in the direction parallel to the rafters. With these assumptions, the shape factors between the roof deck, the rafters and the imaginary surface at the bottom of the rafters through which energy must travel (Fig. 2) could then be easily calculated using the Hottel Cross String Method [7].

Re-radiation between the roof deck and the sides of the rafters creates an effective resistance to radiant heat transfer. This resistance is a function of the emissivities of the roof deck, attic floor and the geometric shape factors between the surfaces. The approach used to account for the radiative resistance was to calculate an effective emissivity for the roof deck by incorporating the radiative resistances resulting from the emissivity of the roof deck and also the resistance resulting from re-radiation between the roof and rafter surfaces. The emissivity of the attic floor was not included in this effective emissivity. The development of the effective emissivity based on the shape factors between surfaces and the roof emissivity was described by Winiarski [8] and can be calculated as

$$\epsilon_{eff} = \frac{1}{\frac{1}{\epsilon_{roof}} + \frac{1}{1-F_{12}} - 1} \tag{1}$$

where ϵ_{eff} refers to the emissivity of the roof deck material and F_{12} refers to the shape factor between the roof deck

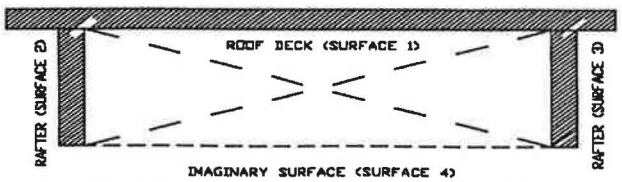

Fig. 2. Roof deck surface and rafters (not to scale).

surface and the inside of a rafter. The effective emissivity was calculated with the assumption of infinite parallel surfaces. Each rafter–roof deck section was actually of a finite length with some radiation leaving the deck and passing out between the ends of the rafters, but not striking the imaginary surface. It was possible to estimate how long each rafter had to be to approximate an infinite surface, by calculating the shape factors between all surfaces for a system of finite length rafters and assuming that radiation leaving the ends of the system passed through two imaginary surfaces at those ends. With these assumptions, the equation for the effective emissivity was identical to Eq. (1) except for replacing F_{12} for the infinite length system with F_{12} for the finite length system. Assuming a base roof deck emissivity of 0.80 as suggested by Sharma and Sharma [9], and 3.8 cm (1.5 in.) by 14 cm (5.5 in.) rafters spaced 0.61 m (24 in.) on center, it can be shown that the difference between the effective emissivity for the actual rafter length and that for the infinite rafter length is less than 2% for a rafter length greater than 1.5 m (4.9 ft).

The shape factors between each of the five attic surfaces were computed by first calculating the shape factor between the attic floor and one roof section and between the two differing roof sections. Shape factor algebra was then used to calculate the shape factors between all other internal surfaces. The first two shape factors were essentially the shape factor between two finite planes joined at a common edge and at an arbitrary angle. The procedure for calculation of this shape factor was described by Hamilton and Morgan [10].

3. Radiation heat transfer

Radiant heat transfer outside the attic was modeled as a simple exchange with an infinite media at a temperature $T_{\text{far out}}$. This temperature was assumed to hemispherically surround the surface, and the radiant energy transfer was calculated as the energy transfer from the surface to a hemispherical black body at $T_{\text{far out}}$ surrounding the surface. For gable and roof surfaces, $T_{\text{far out}}$ must take into account the separate view factors of each surface to the sky (at a calculated sky temperature) and to the surrounding objects which were assumed to be at ambient temperature. For the attic floor, the outside surface was the ceiling of the house. For that surface, $T_{\text{far out}}$ was defined to be the house temperature.

Modeling of radiant heat transfer inside the attic was more complicated due to the re-radiation at each internal surface. The net radiant heat transfer to any surface was modeled using the Net-Radiation Method [7]. The structure of the method used was to present an equation for each surface that related the radiosities of that and the surrounding surfaces to the temperature of that surface in the form

$$\sum_{j=1}^{N} \frac{1}{\epsilon_k} [\delta_{kj} - (1-\epsilon_k) F_{kj}] q_{o,j} = \sigma T_k^4 \tag{2}$$

The five equations of this form, one for each attic surface, were set up in a five-by-five matrix equation of the form

$$[X] \cdot [q_{o,j}] = [\sigma T_k^4] \tag{3}$$

with each element X_{kj} of the form

$$X_{kj} = \frac{1}{\epsilon_k} [\delta_{kj} - (1-\epsilon_k) F_{kj}] \tag{4}$$

Once the matrix [X] was created, the matrix was inverted to form a second matrix [Ψ]. Once inverted, the radiosities of each surface were calculated as

$$q_{o,k} = \sum_{j=1}^{N} \Psi_{kj} \sigma T_j^4 \tag{5}$$

Once the radiosities were calculated, the values for the net radiation given off from each surface was calculated as

$$q_k = \frac{\epsilon_k}{1-\epsilon_k} [\sigma T_k^4 - q_{o,k}] \tag{6}$$

Substituting (5) into (6) yielded

$$q_k = \frac{\epsilon_k}{1-\epsilon_k} [\delta_{kj} - \Psi_{kj}] \sigma T_j^4 \tag{7}$$

An advantage of this technique was that for a specific attic with given dimensions and surface emissivities, the matrix needed to be inverted only once. From then on, the net radiation from any surface was calculated as a function of the inside surface temperatures only.

Eq. (1) involved the surface temperatures to the fourth power. To solve all energy balance equations simultaneously in a linear matrix, it was necessary to expand this equation through a first-order Taylor series about each temperature. This expanded equation was then included in the heat balances for each surface using a Newton–Raphson procedure. The partial derivatives in the expanded equation were evaluated numerically at temperatures from the program's previous iteration.

4. Attic convective heat transfer and air circulation

For each outside and inside attic surface, an air temperature next to that surface was defined. For the outside of the roof and gable sections, the air temperature next to the outside surface was the ambient temperature at the hour examined. For the house ceiling (underside of the attic floor), it was the specified room temperature. For the inside of the attic, a two-zone model for the air temperature was used. Ambient air was assumed to enter the attic through soffit venting along the attic edges and flow in a thin layer along the attic floor. Work by Wolfert and Hinrichs [11] suggested that in a house equipped with soffit venting, 70% of the total volume of air inside an attic flows within 10 cm (4 in.) of the attic floor at low outdoor wind velocities.

Heat transfer occurs between the entering air and the floor. A differential equation was derived for the incremental change in air temperature as it flows along the attic floor.

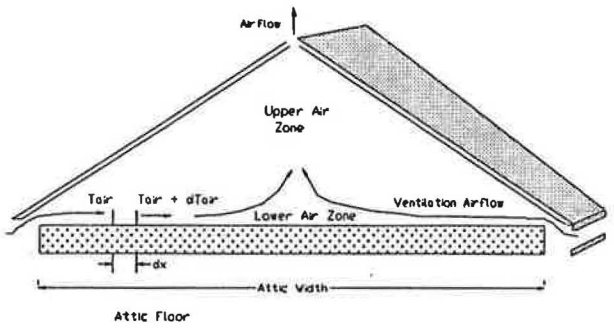

Fig. 3. Attic airflow pattern (model).

Treating the floor as an isothermal surface, one can see (Fig. 3) that for a small distance of travel of the air film in the direction x, the heat balance can be approximated as

$$\int_{T_{\text{entering}}}^{T_{\text{air final}}} M_{\text{air}}\, c_{\text{p}}\, \mathrm{d}T_{\text{air}} = \int_{0}^{L} h_{\text{conv}} W x (T_{\text{floor}} - T_{\text{air}})\, \mathrm{d}x \tag{8}$$

where W was the width of the air film perpendicular to the direction of travel. The limits for the integration are for the length of travel x, 0 to L. For T_{air}, the limits were between the entering temperature, assumed to be ambient, and the final temperature of the air film as it reaches the position L.

By symmetry it was assumed that the final air temperature occurred at a point midway across the width of the attic where the air from the lower zone would rise into the upper attic air zone. Solution of the integral gave the final temperature of the air zone at that point as

$$T_{\text{air final, Zone 1}} = T_{\text{floor}} + (T_{\text{amb}} - T_{\text{floor}}) \times \exp\left[\frac{-h_{\text{conv}}\, WL}{M_{\text{air}}\, c_{\text{p, air}}}\right] \tag{9}$$

This result was identical to that obtained by allowing the entire mass flow of air to travel the length of the attic. This would be similar to the case of cool, wind blown air entering the attic through one gable vent, sinking to the floor, and traveling across the floor until reaching the other end of the attic.

The average difference between the air temperature and the floor temperature for the entire attic floor was found by integrating the difference between the air temperature at some point x and the temperature of the floor (a constant) for the entire length of air travel and then dividing by the length of travel. The average temperature difference across the floor of the attic is then used in calculating the average natural convection coefficient across this surface.

As air leaves the floor of the attic, it moves into the upper air zone. Heat transfer occurs between the upper air zone and the gables and roof sections. To determine a final temperature for this zone, an energy balance was performed on the upper air mass. Both the roof sections and the attic gables are assumed to interact with an average temperature between the entering and the final air temperatures in this zone. Air leaving the attic exits from this upper air zone at this final air temperature.

Natural convection coefficients (in $\mathrm{W/m^2\ K}$) were estimated for all surfaces based on the surface temperature, the air temperature about the surface, and the orientation of the surface with regard to temperature [2]:

$$h_{\text{n}} = A(\Delta T)^{0.33} \tag{10}$$

where

ΔT = temperature difference between surface and the bulk air temperature (K);

$A = 1.52$ for horizontal surfaces facing upward when heated or downward when cooled;

$A = 0.59$ for horizontal surfaces facing downward when heated or upward when cooled;

$A = 1.31$ for vertical surfaces.

The natural convection coefficient for inclined surfaces was assumed to vary linearly with the cosine of the slope of the surface between the extremes of horizontal and vertical surfaces.

The average temperature difference between the floor and the flow of air across the floor is calculated by solving the energy balance equation derived for the floor in Eq. (8) for the temperature difference at position x, multiplying by a differential length $\mathrm{d}x$, and then integrating over the length of travel. The average temperature difference can be found by dividing the result of this calculation by that length of travel. This result was used to calculate the natural convection coefficient for the floor. For the other surfaces, the bulk temperature of the adjacent air mass was used to determine the temperature difference.

The forced convection components on each surface were estimated using the test results by Parmelee and Huebscher [12]:

$$h_{\text{f}} = 5.66 V^{0.8} L^{-0.2} \tag{11}$$

where

V = air velocity (m/s);

L = surface length in direction of air travel (m).

A mixed convection coefficient was calculated for each surface by taking the cube root of the sums of the cubes of the forced and natural convection components at each surface as suggested in Ref. [13].

5. Conduction heat transfer

All conduction heat transfer was assumed to occur as a one-dimensional steady-state process and calculated by dividing the temperature difference across the attic component by the thermal resistance of that component. Residential attics are typically thermally light, with no internal energy generation and little to no massive structural components. Comparison of steady-state and transient finite difference heat transfer models for the attic floor by Winiarski [8] suggested that there would be some time lag and heat flow reduc-

tion effects in that component; however, over daily heat flow cycles, the effect will be small. A time lag of approximately one hour can be expected between the peak heat flow through the attic insulation calculated by a steady-state model and the actual peak heat flow [8]. The results suggested that total daily heat transfer should be within 5% of that predicted using a more complex, finite difference method. As most weather data available for modeling is subdivided into one hour periods, characterization of dynamic heat fluxes at smaller time scales was not a significant consideration in model design. In addition, because the available weather data represent average conditions over each one hour period, the error introduced by assuming steady-state heat transfer as compared to more complex, transient analysis methods, was small.

6. Modeling of radiant barrier types

Three different radiant barriers configurations were used in residences: mounting the radiant barrier directly to the underside of the roof deck (the deck radiant barrier or DRB configuration), placing the radiant barrier horizontally atop the attic insulation (horizontal radiant barrier or HRB configuration), and affixing the radiant barrier to the underside of the roof rafters or trusses (truss radiant barrier or TRB configuration). A modeling technique was developed for each barrier.

For the deck mounted radiant barrier the emissivity of the plywood surface of the attic deck was changed to that of the installed radiant barrier. No change was assumed in the rafter emissivity, and the effective resistance of the roof deck–rafter system was calculated as previously.

Modeling of the horizontal radiant barrier required changing the emissivity of the attic floor and adding a small resistive component to the floor insulation. Observation of the draping of actual horizontal radiant barrier installations suggested an extra air film averaging 0.8 cm (0.32 in.) thick was created because of the inability of the radiant barrier to drape smoothly over the rough surface of the insulation. An extra air film of this thickness was assumed in the horizontal radiant barrier model to lie between the radiant barrier and the insulation surface. Robinson et al. [14] showed that the resistance across such a thin airspace can be calculated by treating radiation and conduction of heat as parallel paths for heat transfer within the airspace and neglecting any convection effects, and this was the approach used in modeling heat transfer across this air layer. The actual thickness of the air film would depend on radiant barrier installation and type of radiant barrier material used.

Modeling of the truss radiant barrier was more complicated than with the other two barrier types. Mounting the radiant barrier on the truss created a second air zone above the barrier but below the attic deck. This air zone was also divided into separate pockets by the presence of the rafters. In the model, it was assumed that this air layer was a sealed airspace with a thickness equal to the height of the rafters and enclosed by two parallel planes at a slope equal to the roof slope. The validity of the sealed airspace assumption would depend on whether a ridge vent system was incorporated into the attic. A combined conduction–convection coefficient was developed for this space by fitting empirical data from Robinson et al. [14]. The data were available for heat transfer between surfaces of 90, 45 and 0° from horizontal, for both heat flow up and heat flow down, as a function of Grashof numbers and plate spacing. In the model, the data were fit over the range of the Grashof numbers likely to be encountered for both the 45 and 0° systems. The coefficient was then assumed to vary linearly with the cosine of the slope of the surface between these two extremes. Roof slopes of greater than 45° are not modeled in this method. The Grashof number was defined as

$$\mathrm{Gr}_L \equiv \frac{g\beta(T_{\mathrm{deck}} - T_{\mathrm{RB}})L^3}{\nu^2} \tag{12}$$

where the values of $g\beta/\nu^2$ were calculated using an air temperature midway between the deck and TRB temperature. From the Robinson data, the Nusselt numbers were of the form:

$$\mathrm{Nu}_\theta = A\,\mathrm{Gr}^B \tag{13}$$

The values of A and B were as shown in Table 1.

For heat flow down at 0° the best fits were obtained using linear relations of the form

$$\mathrm{Nu}_{0°,\,\mathrm{down}} = C\,\mathrm{Gr} + D \tag{14}$$

where the coefficients C and D depended on the range of the Grashof number. Two different ranges can fully describe the Nusselt number for downward heat flow using the coefficients in Table 2. For an arbitrary angle between 0 and 45°, the Nusselt number was assumed to vary linearly with the cosine of the angle between horizontal and 45°.

Robinson et al. [14] also included the stipulation that the resistance to pure conduction always be greater than the resistance to the combined conduction–convection coefficient. In other words, the Nusselt number must always be greater than one. If the value of the Nusselt number was less than one in the calculations, then it was set equal to one. The combined

Table 1
Constants for Eq. (13)

Angle (°)	Direction of heat flow	A	B
0	up	0.100	0.313
45	up	0.0528	0.315
45	down	0.0818	0.321

Table 2
Coefficients for Eq. (14)

Grashof number	C	D
$\mathrm{Gr} < 10^6$	1.28×10^{-7}	1.245
$\mathrm{Gr} > 10^6$	2.80×10^{-7}	1.073

resistance because of the convection–conduction coefficient was then,

$$R_{\text{cond, conv}} = \frac{L}{k_{\text{air}}\,\text{Nu}} \tag{15}$$

7. Environmental modeling

Input data for the model consisted of attic data and time and hourly weather data. Attic data were in the form of the attic dimensions (length, width, height), emissivities of the attic surfaces to IR radiation, absorptivities of the attic surfaces to solar radiation, and the steady-state thermal resistances of each attic component. The hourly data inputs for the model were year, month, day, extraterrestrial solar flux, horizontal solar flux, ambient temperature, dew-point temperature, and wind speed.

The measured incident horizontal radiation was broken into beam and diffuse components using an hourly clearness index k_t and correlations developed by Erbs et al. [15]. Geometric relationships described in Duffie and Beckman [16] were then used to calculate the ratio of the beam radiation on horizontal to the beam radiation on the surface in question; with that ratio, the beam radiation on that surface was calculated. The total solar radiation on any surface was calculated as the sum of the beam radiation on the surface and the diffuse radiation.

Hourly sky temperature is calculated using an approximation of a technique developed by Martin and Berdahl [17] that describes the monthly clear sky emissivity as a function of the dew-point temperature.

$$\epsilon_{\text{cs}} = 0.711 + 0.56\left(\frac{T_{\text{dp}}}{100}\right) + 0.73\left(\frac{T_{\text{dp}}}{100}\right)^2 + 0.013\cos\left(2\pi\frac{t}{24}\right) \tag{16}$$

where

T_{dp} is the dewpoint temperature (°C);

t is the hour of the day ($t=0$ at midnight).

The last term in Eq. (16) was a diurnal correction. The presence of cloud cover increases the total sky emissivity, which has the effect of raising the perceived sky temperature. The sky emissivity with clouds was expressed as

$$\epsilon = \epsilon_{\text{cs}} + (1-\epsilon_{\text{cs}})n\epsilon_{\text{c}}\Gamma \tag{17}$$

where n was the fraction of the sky obscured by clouds, ϵ_{c} was the hemispherical cloud emissivity (set equal to 1), and Γ was a derived factor that depends on the cloud base temperature. For this program, values for Γ were chosen on a monthly basis from a table of values established in Martin and Berdahl for San Antonio, TX [17]. Once the sky emissivity, ϵ, was known, the hemispherical sky temperature is calculated as

$$T_{\text{sky}} = \epsilon^{0.25} T_{\text{air}} \tag{18}$$

where T_{air} is measured in Kelvin.

8. Numerical solution

The attic model resulted in a system of 12 equations that were solved simultaneously for each hour. The equations were as follows: for each outward-facing surface i, energy transfer to the surface from solar radiation, thermal radiation and convection was set equal to the conduction heat transfer across the surface. In equation form, this was

$$\frac{T_{i,\text{outside}} - T_{i,\text{inside}}}{R_i} = \alpha q_{i,\text{sol rad}} + h_{i,\text{rad}}(T_{i,\text{far out}} - T_{i,\text{outside}}) + h_{i,\text{conv}}(T_{\text{amb}} - T_{i,\text{outside}}) \tag{19}$$

For each inside surface i, the conduction heat transfer across the surface was set equal to the sum of the convection heat transfer from that surface and the radiation heat transfer from that surface. The radiation heat transfer was dependent on the temperature of the other inside surfaces and was linearized using the Newton–Raphson technique described previously. The final equation for the heat balance on each inside surface was

$$\frac{T_{i,\text{outside}} - T_{i,\text{inside}}}{R_i} = h_{i,\text{conv}}(T_{i,\text{inside}} - T_{i,\text{air}}) + q_{i,\text{rad old}} + \sum_{j=1}^{5}\frac{\delta q_{i,\text{rad old}}}{\delta T_j}(T_j - T_{j,\text{old}}) \tag{20}$$

For the five interior attic surfaces, this gave 10 equations. There were then two heat balance equations for the two air zones. For the lower air zone, the energy balance was solved implicitly in Eq. (9). For the upper air zone, the energy balance was

$$M_{\text{air}}c_{\text{p, air}}(T_{\text{final, zone 2}} - T_{\text{final, zone 1}}) = \sum_{i=1}^{4} A_i h_i (T_{\text{inside},i} - T_{\text{air},i}) \tag{21}$$

where the summation was over the four roof deck and the gable surfaces and $T_{\text{air},i}$ is equal to $1/2(T_{\text{final, zone 1}} + T_{\text{final, zone 2}})$.

The 12 temperatures solved were the inside and outside surface temperatures of each of the five attic surfaces as well as the final air temperature of the lower and upper attic air zones. An iterative solution was used to account for changes in the convection and radiation coefficients as well as the change in the partial derivatives of the radiation equation at different temperatures. Iterations were completed when the change in each surface temperature between iterations was less than 0.056°C (0.1°F). Initialization of the model for a computer run required inputs of the attic dimensions, orien-

tation, location, emissivities and absorptivities of attic surfaces, and thermal resistances of the attic components. It also required seeding the model with estimated temperatures for each surface in the hour-by-hour solutions. Predictions from this model are compared with experimental results in the next few sections.

9. Experimental setup

Experimental work to validate the model was carried out using two one-room, 3.7 m by 3.7 m test houses located at the Texas Engineering Experiment Station's Energy System Laboratory in Bryan, TX. Each room measured 2.4 m high from floor to ceiling, and the walls of each structure were constructed of 3.8 cm (1.5 in.) by 14 cm (5.5 in.) studs and insulated with fiberglass insulation to a thermal resistance value of 3.35 $m^2°C/W$ (19 Btu/hr-ft^2-F). Both buildings sat on the same concrete slab with one test house (House A) situated approximately 6 m (20 ft) due west of the other (House B).

An attic space was located on the top of each structure. Each attic was gable-ended with the ridge lines running east–west. The roof of each attic structure was supported by 3.8 cm (1.5 in.) by 14 cm (5.5 in.) rafters spaced 60 cm (24 in.) on center. The roof decking was made of 1.3 cm (0.5 in) thick plywood and was covered with tarpaper and shingled. Although originally dark, the shingles had been weathered to a light gray. The house ceiling was 1.3 cm (0.5 in.) gypsum board and was attached to 5 cm (3.8 in.) by 15 cm (5.5 in.) ceiling joists spaced 60 cm (24 in.) on center. Dampered fan units located at the top of the east gable of each house were used for ventilation. Experimentally derived fan curves for each fan related the airflow rate to the pressure drop across each fan's damper. This allowed the airflow rate to be set during each test. The air inlets for each attic were at the base of the west attic gable and consist of narrow slits 3.8 cm (1.5 in.) high by 3 m (10 ft.) wide. These slits were located approximately 7.6 cm (3 in.) above the top of the floor joists.

Cooling for each structure was accomplished with a chilled water/glycol solution circulated through a single fan coil unit in each house. Resistance heating was used for each house during winter heating tests. Inside temperatures for both houses were held to within 0.5°C (0.9°F) of each other at all times during the tests.

10. Instrumentation

Approximately 120 sensors were installed in each house. Shielded type-T thermocouple grids were used to measure the temperature of the indoor room, ceiling, roof deck, roof truss and shingles, as well as ambient temperature. An internal grid of thermocouples was used to measure air temperature at four different levels across the length of the attic. A smaller grid was used for selected tests to measure temperature at three different levels inside the attic insulation. Type-T thermocouples are typically accurate to within 0.5°C.

To measure heat flux through the attic ceiling, five 10 cm × 10 cm (4 in. × 4 in.) heat flux meters were located on the ceiling of each house. Four meters were placed between the floor joists, and one meter was mounted directly below a floor joist. Each heat flux meter had a rated accuracy of 1%. A pyranometer was used to measure the total horizontal solar radiation. Heat flux and temperature data were recorded at one-minute intervals and integrated over each one-hour period using a data logger. To calculate house energy use, turbine flow meters measured the flow of cooling water to each house while thermocouples recorded the temperature drop across the fan coil unit every 10 s during the on-time of each pump.

11. Tests

The four tests reported here consisted of side-by-side comparisons of radiant barrier (RB) performance during summer conditions. The tests consisted of comparisons of the no radiant barrier (No RB), and truss radiant barrier (TRB) test cases for three differing nominal values of insulation, 1.93, 3.35 and 5.29 $m^2°C/W$ (11, 19 and 30 Btu/hr-ft^2-F, respectively) and one side-by-side comparison of the truss radiant barrier (TRB) and horizontal radiant barrier (HRB) configurations for a 3.35 $m^2°C/W$ (19 Btu/hr-ft^2-F) insulation level. The tests focused on the truss radiant barrier configuration as it was felt that that was the most practical retrofit for most residences. Timing and weather conditions did not allow a test of the deck mounted radiant barrier (DRB) configuration during the test period. The insulation used in each case consisted of unfaced fiberglass batts, and the airflow in the attic was maintained at a constant 0.305 $m^3/min\text{-}m^2$ (0.25 $ft^3/min\text{-}ft^2$). The test periods, house configurations and environmental conditions are described in Table 3.

The radiant barrier material used for the tests consisted of an aluminized sheet of synthetic material bonded to a reinforcing fiber mesh backing. The material was perforated, with the perforations accounting for approximately 2% of the area of the radiant barrier. The emissivity of the aluminized surface was measured using an emmissometer to be 0.04. The emissivity of the perforations was assumed to be 1.00. The emissivity of the radiant barrier was calculated as the area average of the two emissivities or

$$\epsilon_{RB} = 0.98\epsilon_{Al} + 0.02\epsilon_{Perf} \quad (22)$$

yielding an estimated barrier emissivity of 0.06.

During Tests 2, 3 and 4, the temperature of the top surface of the insulation was measured along with the room ceiling temperature. These measurements made it possible to compare the measured values for heat flux directly with the temperature drop across the insulation on an hour-by-hour basis. A linear regression was done on these measurements to esti-

Table 3
Test periods and conditions

Test	Test period	Nominal base insulation ($m^2°C/W$)	House configuration	Av. T_{indoor} (°C)	Av. $T_{ambient}$ (°C)	Daily solar insulation (kJ/m^2)
1	July 01–July 6	1.93	(A) R-11 No RB (B) R-11 TRB	(A) 23.1 (B) 23.0	33.2	27300
2	July 08–July 14	3.35	(A) R-19 No RB (B) R-19 TRB	(A) 23.1 (B) 23.0	33.8	26850
3	July 15–July 20	5.29	(A) R-30 No RB (B) R-30 TRB	(A) 23.1 (B) 23.0	34.3	24530
4	July 22–July 26	3.35	(A) R-19 No RB (B) R-19 TRB	(A) 23.1 (B) 23.0	33.2	23200

Table 4
Floor resistances

Test	House	Floor resistance ($m^2°C/W$)		
		w/o stud nominal	w/o stud regressed	with stud calculated
1	A	2.02	N.A.	1.90
	B	2.02		1.90
2	A	3.43	3.17	2.77
	B	3.43	3.30	2.87
3	A	5.37	4.46	3.61
	B	5.37	4.47	3.61
4	A	3.43	2.96	2.63
	B	3.43	3.03	2.68

mate the steady-state resistance for the insulation. Because of the much greater thermal lag occurring in the floor joist, only the average heat flux measured by the heat flux meters directly under the insulation was used in this analysis. Table 4 shows the nominal and experimentally determined resistance value for each test. The regressed values for thermal resistance were less than the nominal values supplied by the manufacturer.

To calculate the total ceiling resistance including the floor joists, the fraction of joist area was included as a parallel path for heat transfer along with the regressed value for the insulation. If the regressed value was not available, the nominal resistance value was used. The resistance used for the softwood joists was assumed to be 1.06 $m^2°C/W$. The calculated resistances including the joists are also shown in Table 4.

12. Experimental and model results

The primary variables considered in determining how well the model simulated the attics included shingle temperature, hourly heat flux values through the ceiling, and the overall energy flow through the ceiling for each test period.

Shingle temperature was considered to be the deciding factor in how well the environmental conditions were being modeled. Experimental results from side-by-side tests of one house with and one house without a radiant barrier showed that shingle temperatures for the houses were essentially identical for any particular hour of interest. This can be clearly seen in Fig. 4 and suggested that the shingle temperature was not greatly influenced by the energy flow beneath the shingle, but rather reflected the outside environmental conditions. Comparison of measured shingle temperatures and model predictions for Test 2 can be seen in Fig. 5 and Fig. 6 for the TRB and No RB cases, respectively. Model predictions suggested average peak shingle temperatures of from 1 to 2°C higher in the house with the TRB as compared to the No RB configuration.

The ability to predict hourly heat fluxes through the house ceiling was a basic goal of the model. Fig. 7 shows hourly heat flux predictions along with measured data for one day during Test 2. The predictions shown were for the average

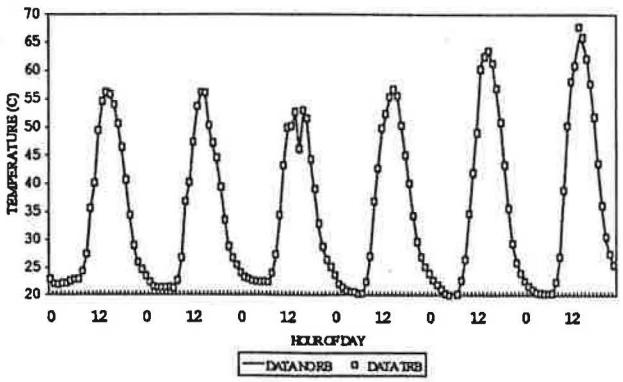

Fig. 4. Measured shingle temperatures for two houses in Test 2.

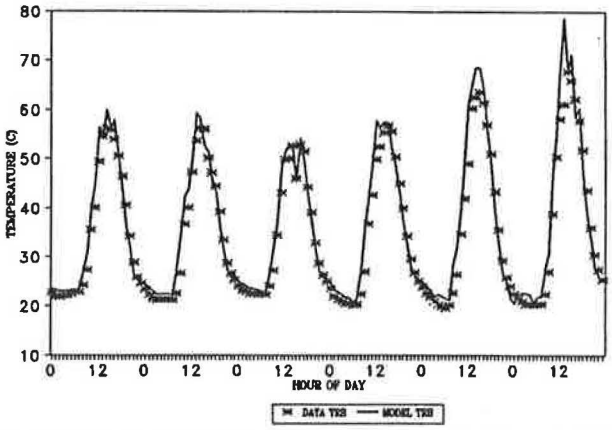

Fig. 5. Measured and model shingle temperatures for House A, TRB, Test 2.

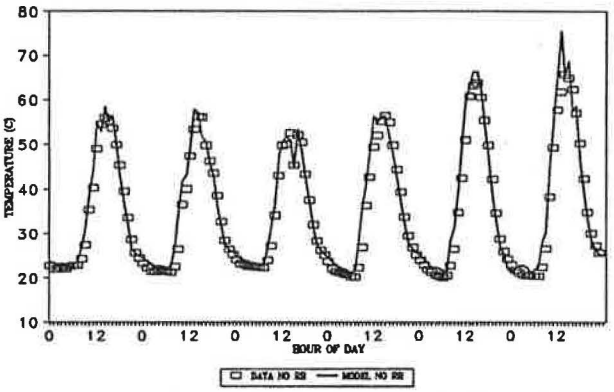

Fig. 6. Measured and model shingle temperatures for House B, No RB, Test 2.

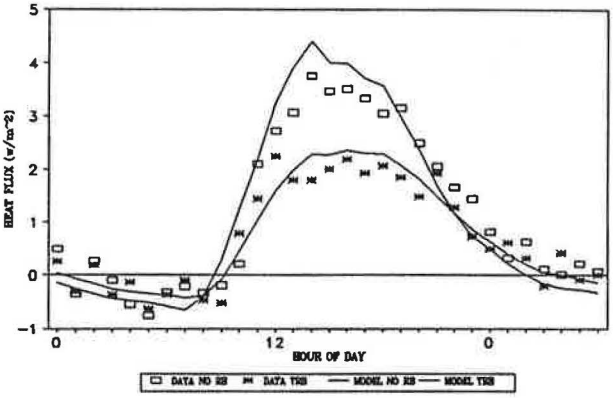

Fig. 7. Heat flux results from Test 3.

heat flux underneath the insulation and did not include heat flow through the floor joist. The predictions have been smoothed using a rolling average technique and shifted by one hour to allow for the thermal lag in the floor system, as discussed previously. The model tended to overpredict the peak daytime flux for both the No RB and TRB test cases. In Test 2 (3.35 m^2 K/W (19 Btu/hr-ft^2-F) insulation), peak heat fluxes in the No RB case averaged approximately 6% higher in the model than in the test data. Greater disparity was seen in the TRB case, where predicted peak heat fluxes averaged approximately 14% higher than were measured. In addition, in the tests examined, the model tended to either slightly underpredict the nighttime heat flux into the house or predicted a small heat flux going out of the house when none was present in the measured data. This is likely due to the model's inability to correctly account for residual heat leaving the attic at night.

Comparison of the HRB and TRB cases (Test 4) showed a greater reduction in intergrated heat flux with the HRB as compared to the TRB configuration. Over the test period, the total ceiling heat transfer in the house outfitted with the HRB was 5.8% lower than it was in the house with the TRB. The difference in integrated heat flux suggested by the model was less than 1% between the two houses, with the HRB configuration showing the lower ceiling heat flux.

Table 5 shows the integrated heat flux for all tests as compared with the model predictions. These results are for the average heat flux through the entire ceiling including the attic floor joists. In all summer tests, the model underestimated the heat flow down through the ceiling (shown as a negative heat flux). Agreement was best in Tests 2, 3 and 4 where the experimental value of thermal resistance was used. Inclusion of the floor joist in the model lowered the thermal resistance of the floor and consistently raised the predicted effectiveness of the radiant barrier (expressed as the percentage reduction in heat flow over the No RB case). Examination of the measured data showed that the measured radiant barrier effectiveness did not always increase when the area under the floor joist was included in the heat flux measurement.

13. Uncertainty analysis

This section deals with the sensitivity of the model predictions to some of the key physical characteristics of the test houses. It was desired to determine the parameters whose uncertainty had the greatest impact on the net summer heat flux and on the percentage reduction in heat flux caused by a radiant barrier. These results then determine the accuracy to which these parameters must be known for a given degree of certainty in the final ceiling heat flux. This information should prove useful in developing future, more elaborate modeling efforts or evaluating past efforts.

Several house parameters were either estimated in the development of the model or were measured in the test houses with a limited degree of accuracy. It is important to examine how a change in these parameters can affect the predicted ceiling heat flow and the reduction in the ceiling heat flow caused by the radiant barrier. The physical parameters believed to have the largest influence on the model predictions are listed in Table 6 along with a base value for that parameter and an estimate of the uncertainty associated with that parameter. The uncertainty estimates were determined either from a review of available literature with estimated values for the parameter or from estimates made during the course of the experimental study.

Table 5
Tabulated experimental and model heat flux results

Test	House	Radiant barrier configuration	Daily ceiling load (kJ/m²)		Integrated reduction (%)	
			Experimental daily ceiling	Predicted daily ceiling	Experimental	Predicted
1	A	No RB	327	274	37	43
	B	TRB	207	158		
2	A	No RB	240	224	38	39
	B	TRB	149	136		
3	A	No RB	175	167	29	35
	B	TRB	125	109		
4	A	HRB	130	108	6	1
	B	TRB	138	109		

Table 6
Heat flow sensitivity analysis

Parameter	Base value	Uncertainty	Heat flow uncertainty		
			No RB	HRB	TRB
Floor resistance	2.91 m² K/W	± 10%	8.9%	7.5%	7.9%
Roof convection	various	± 25%	5.4%	1.5%	1.5%
Roof absorptivity	0.70	± 0.08	2.8%	1.3%	1.0%
Floor convection	various	± 25%	2.3%	0.4%	0.5%
Airflow rate	0.305 m³/min m²	± 5%	0.6%	0.0%	0.1%
Insulation emissivity	0.85	± 0.10	0.6%	0.0%	0.0%
Deck emissivity	0.80	± 0.05	0.5%	0.1%	0.0%
Radiant barrier emissivity	0.06	± 0.02	N.A.	5.2%	5.2%
Airspace created by HRB	0.8 cm	± 0.5 cm	N.A.	4.3%	N.A.
Airspace created by TRB	15 cm	± 2.0 cm	N.A.	N.A.	0.5%

Sensitivity analysis was carried out by running tests for a single-day period on 12 July 1991, using measured climatic data. Two model runs were used to establish a daily integrated heat flow value for both the No RB test case and the HRB test case with all variables at their base value. Next, for each attic configuration, a run was made with each parameter at its upper and at its lower uncertainty value and all other parameters held at the base case value. By normalizing the total daily heat flow at the new parameter values to that of the base case, the uncertainty in heat flow because of that parameter was established. Table 6 shows the average estimated uncertainty in daily heat flow that results from the uncertainty in these parameters. Results of this analysis pointed to the uncertainty in the floor thermal resistance as having the largest effect on heat flow in all attic configurations. Uncertainty in the roof convection coefficient had a large effect in the No RB configuration but small effects in both radiant barrier configurations. Changes in radiant barrier emissivity showed large effects on both radiant barrier configurations. The uncertainty in the airspace thickness beneath the HRB also had a large effect on the total heat flow for that configuration. Variation in all other parameters had less than a 3% change in the daily ceiling heat flow in all house configurations.

Data from the above sensitivity analysis were also used to determine the effect of varying the above parameters on the percentage heat flow reduction produced by the radiant barrier. For the day in question, the predicted heat flow reduction produced by the HRB was 37%; that produced by the TRB was 36%. Variation in most of the above parameters had very little effect on that reduction. Those that had the most significant effect are shown in Table 7. The parameters that had the highest effect on the percentage reduction in heat flux were not necessarily those parameters with the highest impact on total heat flux. Instead, they were parameters that had the most disparate influence between attics with and without radiant barriers. Variation in the radiant barrier emissivity had the greatest impact on radiant barrier effectiveness, but this was followed closely by variation in the thickness of the

Table 7
Sensitivity of radiant barrier effectiveness

Parameter	HRB	TRB
Barrier emissivity	3.3%	3.3%
Airspace created by HRB	2.7%	N.A.
Roof convection coefficients	2.4%	2.4%
Floor resistance	0.9%	0.7%

airspace beneath a radiant barrier installed in the HRB configuration. Uncertainty in the airspace created above a radiant barrier in the TRB configuration had little effect. Variation in the roof convection coefficient also had a significant impact on radiant barrier effectiveness because this parameter strongly influenced the roof temperature and thus the radiation from the attic deck. The resistance of the attic floor also had a slightly disparate effect on heat flow between attics with and without radiant barriers, resulting in a small change in predicted radiant barrier effectiveness. All other parameters examined had minor impacts on radiant barrier effectiveness. It was particularly important to note the large change in effectiveness in response to a small change in radiant barrier emissivity. This is a concern of the insulation industry because dust contamination of the radiant barrier surface over time is expected in most installations.

14. Conclusions

Comparisons of model predictions with the experimental results showed good qualitative agreement in roof shingle temperatures and heat flux for all tests. Numerical agreement in integrated heat flow through the ceiling was hampered by the tendency of the model to underpredict off-peak heat flux during the cooling season and overpredict peak daytime heat flux. Predicted radiant barrier effectiveness was between 1 and 6 percentage points higher than that seen in the experimental results. The measured reduction in integrated ceiling heat flux over a one week period with 3.35 m^2°C/W (19 Btu/hr-ft^2-F) was 38%. That predicted by the quasi-steady state model was 39%. The magnitude of the integrated ceiling heat flux prediction was between 83 and 95% of that measured during the experimental studies during all tests.

Sensitivity studies suggested that for most of the parameters examined, the relative change in integrated heat flux resulting from uncertainty in a parameter was significantly less than the relative uncertainty in the parameter. The exception to this was in the thermal resistance of the floor, where these uncertainties were of the same order. A small variation (0.02) in the radiant barrier emissivity was shown to produce a relatively large variation in the predicted integrated heat flux in both horizontal and truss mounted radiant barrier configurations, illustrating the sensitivity to this parameter. Airspaces created between the horizontal radiant barrier and insulation surface were seen to also have significant effects on the integrated heat flux through the attic floor. Variation in these latter two parameters also caused the biggest variation in the modeled radiant barrier effectiveness. In future comparisons between modeling and experimental work, these three parameters (floor thermal resistance, radiant barrier emissivity, and air space between a horizontal radiant barrier and attic floor insulation) should be identified as accurately as possible.

15. Nomenclature

A	surface area (m^2)
c_p	specific heat capacity (kJ/kgK)
DRB	deck radiant barrier
F	shape factor
g	gravitational constant (m^2/s^2)
Gr	Grashof number
h	convective coefficient (W/m^2K)
HRB	horizontal radiant barrier
k	thermal conductivity (W/mK)
k_t	clearness index
L	characteristic length (m)
M	mass (kg)
n	day of year, fraction of cloud cover
Nu	Nusselt number
Q	heat flow (kJ)
q	heat flux (W/m^2)
RB	radiant barrier
t	time (h)
T	temperature (K)
TRB	truss radiant barrier
V	air velocity (m/s)
W	width (m)
X	radiation matrix

Greek letters

α	thermal diffusivity, solar absorptivity (m^2/s)
β	volumetric thermal expansion coefficient (k^{-1})
Δ	difference
Γ	gamma factor for cloud emissivity
δ	partial derivative, kroneker delta
ϵ	emissivity
Ψ	matrix

Subscripts

air	air
amb	ambient
c	cloud
cond	conductive
conv	convective
cs	clear sky
d	diffuse
deck	deck
dp	dew-point
eff	effective
f	forced
floor	floor
h	horizontal
i	outward facing surface
j, k	numerical subscript
L	length
n	natural
o	out

r	radiative
s	sky
solair	solair temperature
solrad	solar radiation

Acknowledgements

This research was sponsored by the State of Texas through the Texas Higher Education Coordinating Board, Energy Research in Applications Program Fund, and the Texas A&M University Energy Systems Laboratory. The authors wish to thank these institutions for their past and continuing support of this project.

References

[1] F.A. Joy, Improving attic space insulating values, *ASHRAE Trans., 64* (1958) 251–266.

[2] *ASHRAE Handbook — 1989 Fundamentals*, ASHRAE, American Society of Heating and Refrigeration Engineers, Atlanta, GA, 1989.

[3] B.A. Peavy, A model for predicting the thermal performance of ventilated attics, summer attic and whole house ventilation, *NBS Special Publication 548*, 1979, pp. 119–149.

[4] K.E. Wilkes, Thermal model of residential attics with radiant barriers: comparison with laboratory and field data, presented at the *Conf. Thermal Performance of the Exterior Envelopes of Buildings IV, Orlando, FL, 1989.*

[5] P.W. Fairey and M. Swami, Analysis of attic radiant barrier systems using mathematical models, *Proc. Fifth Annual Symp. Improving Building Energy Efficiency in Hot and Humid Climates, 1988*, Texas A&M University, pp. 186–193.

[6] P.W. Fairey, M. Swami and D. Beal, RBS technology: Task 3, *Rep. DRAFT*, Sponsored by Florida Power and Light and the US Department of Energy, Florida Solar Energy Center, Cape Canaveral, FL, 1988.

[7] R. Siegal and J. Howell, *Thermal Radiation Heat Transfer*, Hemisphere, New York, 1981.

[8] D.W. Winiarski, A quasi-steady-state model to predict attic heat transfer and energy savings in residences using radiant barriers, *Master's Thesis*, Texas A&M University, 1992.

[9] V.C. Sharma and A. Sharma, Solar properties of some building elements, *Energy, 14* (1989) 805–809.

[10] D.C. Hamilton and W.R. Morgan, Radiant interchange configuration factors, *NACA TN 2836*, 1952.

[11] C.K. Wolfert and H.S. Hinrichs, *Fundamentals of Residential Attic Ventilation*, HC Products Company, Princeville, IL, 1974.

[12] G.V. Parmelee and R.G. Huebscher, Forced convection heat transfer from flat surfaces, *ASHRAE Trans., 53* (1947) 245–284.

[13] F.P. Incropera and D.P. De Witt, *Fundamentals of Heat and Mass Transfer*, Wiley, New York, 1985.

[14] H.E. Robinson et al., The thermal insulating value of airspaces, *Housing Research Paper 32*, US Government Printing Office Washington, DC, 1954.

[15] D.G. Erbs et al., Estimation of the diffuse radiation fraction for hourly, daily, and monthly-average global radiation, *Solar Energy, 28* (1982) 293–302.

[16] J.A. Duffie and W.A. Beckman, *Solar Thermal Energy Processes*, Wiley-Interscience, New York, 1974.

[17] M. Martin and P. Berdahl, Characteristics of infrared sky radiation in the United States, *Solar Energy, 33* (1984) 321–336.